



Article

Assessment of the Blasting Efficiency of a Long and Large-Diameter Uncharged Hole Boring Method in Tunnel Blasting Using 3D Numerical Analysis

Min-Seong Kim ¹, Chang-Yong Kim ¹, Myung-Kyu Song ² and Sean Seungwon Lee ^{2,*}

¹ Department of Geotechnical Engineering Research, Korea Institute of Civil Engineering and Building Technology, 283 Goyang-daero, Goyang-si 10223, Korea

² Department of Earth Resources and Environmental Engineering, Hanyang University, 222 Wangsimni-ro, Seoul 04763, Korea

* Correspondence: seanlee@hanyang.ac.kr

Abstract: Cut blasting is one of the most essential processes to reduce blast-induced vibration in tunnel blasting. The long and large-diameter uncharged hole boring (LLB) method is an example of one of the cut blasting methods, which utilizes large-diameter uncharged holes drilled in the tunnel face. In this study, blasting simulations were performed to analyze its blasting mechanism, and the LLB method and the traditional burn-cut method were simulated to compare their blasting efficiency. A 3D numerical analysis using LS-DYNA code, a highly non-linear transient dynamic finite element analysis using explicit time integration, was used to simulate the blasting process, and a Johnson–Holmquist constitutive material model, which is optimal for simulating brittle materials under dynamic conditions, was used to simulate the rock behavior under blasting. The modified LLB method showed a 3.75-fold increase in the advance per round compared to the burn-cut method, due to the increased formation of long and large-diameter uncharged holes compared to blast holes. This modified LLB method used 30% less explosives, so its failure range was approximately 1.25 times less than that of the burn-cut method, but its advance was approximately 4 times larger than the burn-cut method, which was similar to the original LLB method. This confirmed that the modified LLB method is significantly more efficient in terms of increased blasting efficiency (particularly the advance per round) as well as reduced blast-induced vibration, compared to the traditional cut blasting method.

Keywords: tunnel excavation; cut blasting method; LLB method; uncharged hole; numerical simulation



Citation: Kim, M.-S.; Kim, C.-Y.; Song, M.-K.; Lee, S.S. Assessment of the Blasting Efficiency of a Long and Large-Diameter Uncharged Hole Boring Method in Tunnel Blasting Using 3D Numerical Analysis. *Sustainability* **2022**, *14*, 13347. <https://doi.org/10.3390/su142013347>

Academic Editors: Jian Zhou, Mahdi Hasanipanah and Danial Jahed Armaghani

Received: 14 September 2022

Accepted: 10 October 2022

Published: 17 October 2022

Publisher's Note: MDPI stays neutral with regard to jurisdictional claims in published maps and institutional affiliations.



Copyright: © 2022 by the authors. Licensee MDPI, Basel, Switzerland. This article is an open access article distributed under the terms and conditions of the Creative Commons Attribution (CC BY) license (<https://creativecommons.org/licenses/by/4.0/>).

1. Introduction

A drill and blast method is the most common rock excavation method in mining and civil engineering. However, this method causes environmental pollution and hazards such as noise, vibration, and flying rocks generated by the blasting, and blast-induced vibration can damage nearby structures in urban areas, when it exceeds specific values [1,2]. In tunnel construction, the advance rate is one of the key factors because it is directly related to the overall construction period and influences the economic feasibility of a project. Therefore, the ultimate goal of blast excavation in the new Austrian tunneling method (NATM) is to maximize the advance per round, while meeting the allowable criteria for blast-induced vibration. It is well known that blast-induced vibration is the most significant factor that affects the surrounding structures [3]. In the rock fragmentation caused by blasting, it has been found that only 20–30% of the energy is used in the breakage of the surrounding rocks, while the residual energies are dissipated in the forms of vibration, noise, and flying rocks [4,5]; thus, the current blasting techniques have inevitable limitations [6]. When the vibration exceeds a critical value, internal cracks in the rock mass can be induced, potentially harming nearby structures [7]. Given the recent rise in environmental concerns,

complaints about blast-induced vibration and noise continue to increase, and regulations are becoming commensurately stricter [8].

Several parameters affect blast-induced vibration [9], and the free face is one of the most efficient factors in maximizing the blasting efficiency, as well as reducing vibration. Unlike open-pit mines, tunnel structures generally have only one free face, so the cut blasting method is necessary to create artificial additional free faces to improve the blasting efficiency. V-cuts and burn-cuts, which are the traditional cut blasting methods, are widely used in tunnel blasting. Using the traditional cut method, more explosives are needed to increase the advance, but there are limits to increasing the amount of explosives, while keeping to the allowable limit of vibration.

A long and large-diameter uncharged hole boring (LLB) method is an advanced cut blasting method that involves boring large-diameter uncharged holes. This method has been reported to have significantly less blast-induced vibration than traditional cut methods [10]. The high-performance LLB machine generally drills 50 m with a 382-mm hammer bit at a time, considering the overall working process and drilling time. Thus, this method has the great advantage of creating large-diameter uncharged holes (free faces) that are deeper than regular blast holes, thus significantly increasing the advance per round compared to the traditional cut method [11].

However, the cut methods in tunnel blasting that utilize large-diameter uncharged holes (over 350 mm) have not yet been fully analyzed in terms of failure mechanisms and blasting efficiency. In addition, in some tunnel construction sites where the LLB method was used, the advance per round was similar to, or even less than, the traditional cut methods. In the actual tunnel construction site, if explosive material detonates inside the rock mass, there is a limit to investigating the failure mechanism of the LLB method because an instantaneous explosion reaction occurs. To investigate the failure mechanism of blasting more accurately, experimental studies should be conducted, but several risks and limitations are involved because they are very expensive and time-consuming [12]. Instead, numerical approaches have been widely used to overcome the many limitations of experimental research [13–15].

In this study, a series of numerical analyses were carried out to investigate the failure mechanism of tunnel blasting with the LLB method. The LS-DYNA software, which is a finite element software that can handle dynamic and non-linear problems, was used to simulate the tunnel blasting. The traditional burn-cut method and the LLB method, as employed to create uncharged holes for reducing blast-induced vibration, were modeled, to compare their blasting mechanisms and efficiency, especially the advance per round. Additional analysis was performed to compare the blasting efficiency when a reduced amount of explosives was used with the LLB method.

2. Long and Large-Diameter Uncharged Hole Boring Method

2.1. Introduction to the LLB Method

The LLB method is an advanced cut blasting method to minimize the vibration generated by blasting in a NATM tunnel. This method creates long and large-diameter (382-mm) uncharged holes at a cut area using a high-performance boring machine, as shown in Figure 1. The LLB hole serves to release the confining stresses of the rock mass before blasting. When an explosive detonates in the blast hole, the adjacent uncharged hole can not only provide a larger space for moving breaking rocks, but can also change the stress distribution in the rocks around the uncharged hole, which is called the “uncharged hole effect” [16].

One of the outstanding characteristics of this method is that it typically drills 50 m at a time, and can efficiently drill up to 65 m without any problems. Thus, additional free faces are formed beyond the depth of the blast hole, which theoretically has the advantage of increasing the advance per round. In addition, one to three holes are generally drilled in the LLB method, depending on what is applicable in the site conditions. Unlike the conventional cut blasting methods, such as V-cut and burn-cut, this method is applicable

for both weak and hard rock masses. The field application of the LLB machine and a tunnel face with completed drilling are shown in Figure 2 [10].

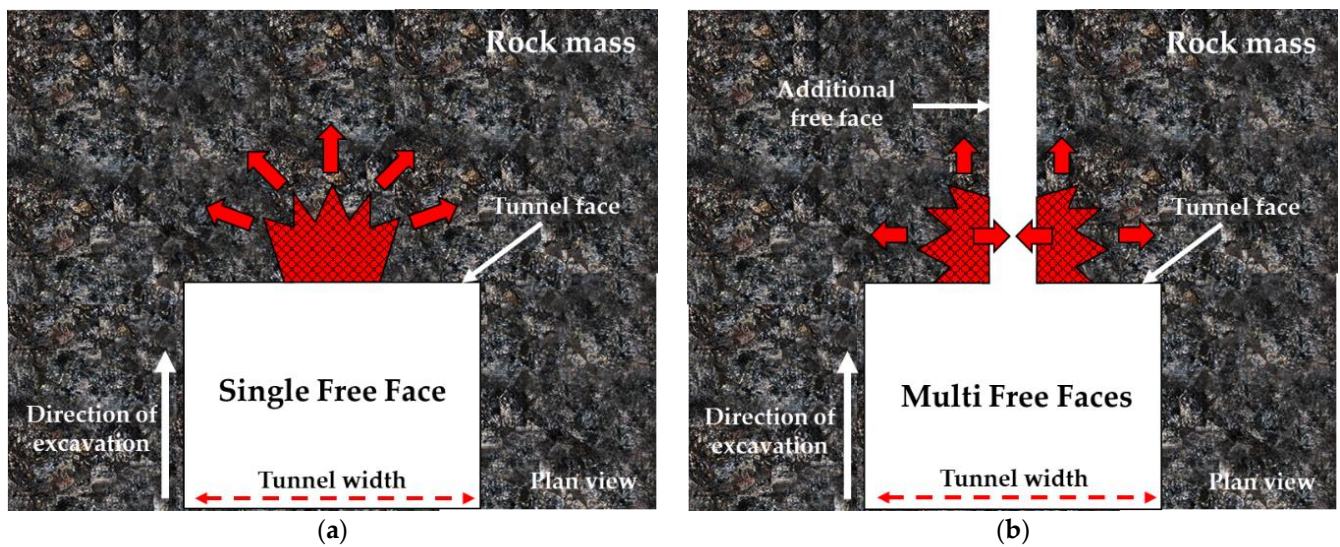


Figure 1. Comparison of general blasting and controlled blasting using the LLB method. (a) General blasting; (b) controlled blasting using the LLB method.



Figure 2. Images of field application of the LLB machine and a tunnel face with completed drilling. (a) Field application of the LLB machine; (b) tunnel face with completed drilling.

2.2. A Mechanism of Tensile Fracturing by Long and Large-Diameter Uncharged Holes

When an explosive detonates in a blast hole, gaseous detonation products fill the blast hole with high pressure and temperature. This high-pressure detonation gas is immediately applied to the surface of a blast hole and generates radial compressive stress, which is generally greater than the strength of the rock [17,18]. The compressive stress wave generated by blasting turns into a tensile stress wave when it reaches a free face, and the reflected tensile wave returns through the rock mass [19–21]. This behavior is generally called the Hopkinson effect, and the principle of this theory is illustrated in Figure 3 [22].

It is well known that the dynamic tensile strength of rock is much lower than the dynamic compressive strength [23,24]. If the tension stress waves exceed the dynamic tensile strength of the rock, cracks will be generated gradually, and this tensile stress leads to greater damage to the rock mass in the vicinity of the free face [16]. Therefore, when a propagated compressive stress wave from the detonated explosive reaches an uncharged hole, it turns into a tensile stress wave; thus, the rock is effectively crushed around the uncharged hole. A tunnel structure generally has only one free face, which is the tunnel

face. To effectively blast in tunneling, adding free faces is the most vital factor for initiating or maximizing the Hopkinson effect.

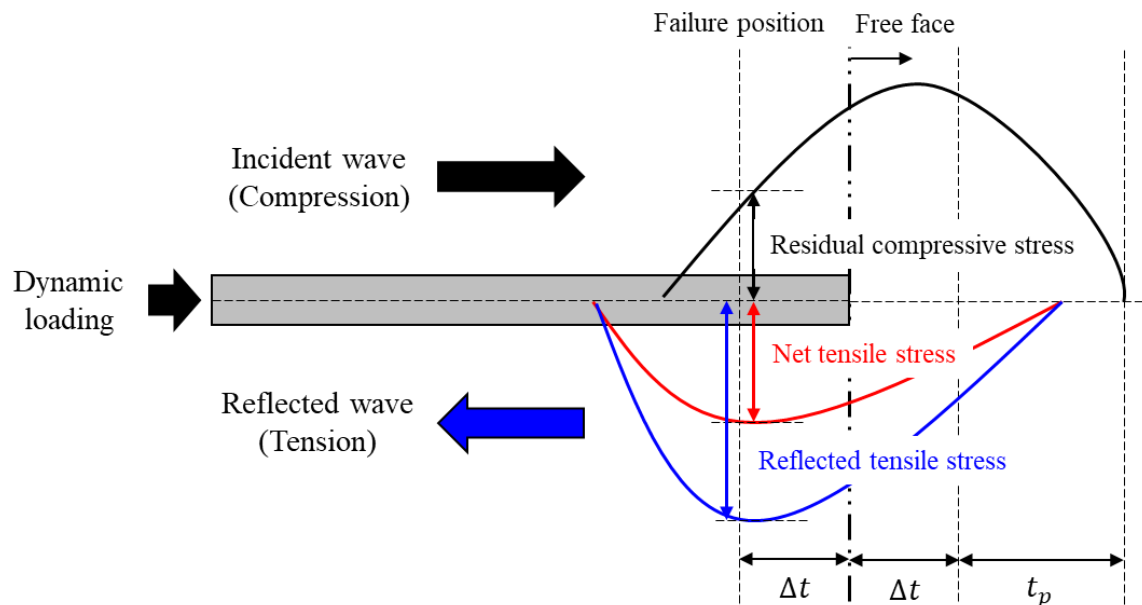


Figure 3. Principle of the Hopkinson effect.

3. Numerical Analysis

3.1. Analysis Model

This study used the LS-DYNA software, which is widely used for blasting simulations, to simulate dynamic and non-linear problems. The arbitrary Lagrangian–Eulerian (ALE) formulation was employed to investigate blast-induced pressure and its interaction with various materials [25–27]. The ALE formulation contains both Lagrangian and Eulerian formulations to utilize the advantages of each approach [28]; it allows the mesh to move independently from the material flow, and each element in the mesh can contain mixtures of different materials [29].

The burn-cut method and the LLB method were modeled to investigate their effects on the blasting efficiency, including the advance per round in tunnel blasting. Both analysis models included the rock, explosives, and stemming in the charge hole, as well as uncharged holes. The rock was modeled using the Lagrangian method, with a geometry of 1500 mm × 1500 mm × 1500 mm to focus on the cut area, as shown in Figure 4. The diameter of the blast holes was 50 mm and they contained 300 mm of explosives and 700 mm of stemming, which were modeled with the ALE method. The diameters of the uncharged holes for the burn-cut and the LLB method were 102 mm and 382 mm, respectively. The spacing between the blast hole and the uncharged hole for the burn-cut was 200–300 mm and 400 mm for the LLB method. The geometries were modeled based on actual design cases from subway tunnel construction sites in South Korea. In both cases, the explosives were set to detonate at the same time, and the boundary conditions were set as non-reflecting boundaries for all sides, except the tunnel face.

3.2. JH-2 Constitutive Model for Rock Material

A Johnson–Holmquist (JH-1) constitutive material model was initially proposed for studying the behavior of metals such as copper and nickel under large strain, high strain rate, and high-pressure conditions. Based on the JH-1 model, an improved material model, named as the JH-2 constitutive model, was suggested to describe the mechanical behavior under dynamic conditions, considering the softening property of brittle materials. The JH-2 model is widely used in LS-DYNA to simulate the dynamic behavior (blasting) of rocks. This improved model represented the strength and damage of material as functions of the

representative variables and the damage evolution within the material was considered. In addition, this model considers the pressure, strain-rate dependent strength, damage, and fracture of materials [30–32]. Granite is one of the most brittle materials and a widely distributed underground rock material in South Korea. Therefore, granite properties were used here to simulate the tunnel blasting, as shown in Table 1 [33]. A general overview of the model is illustrated in Figure 5.

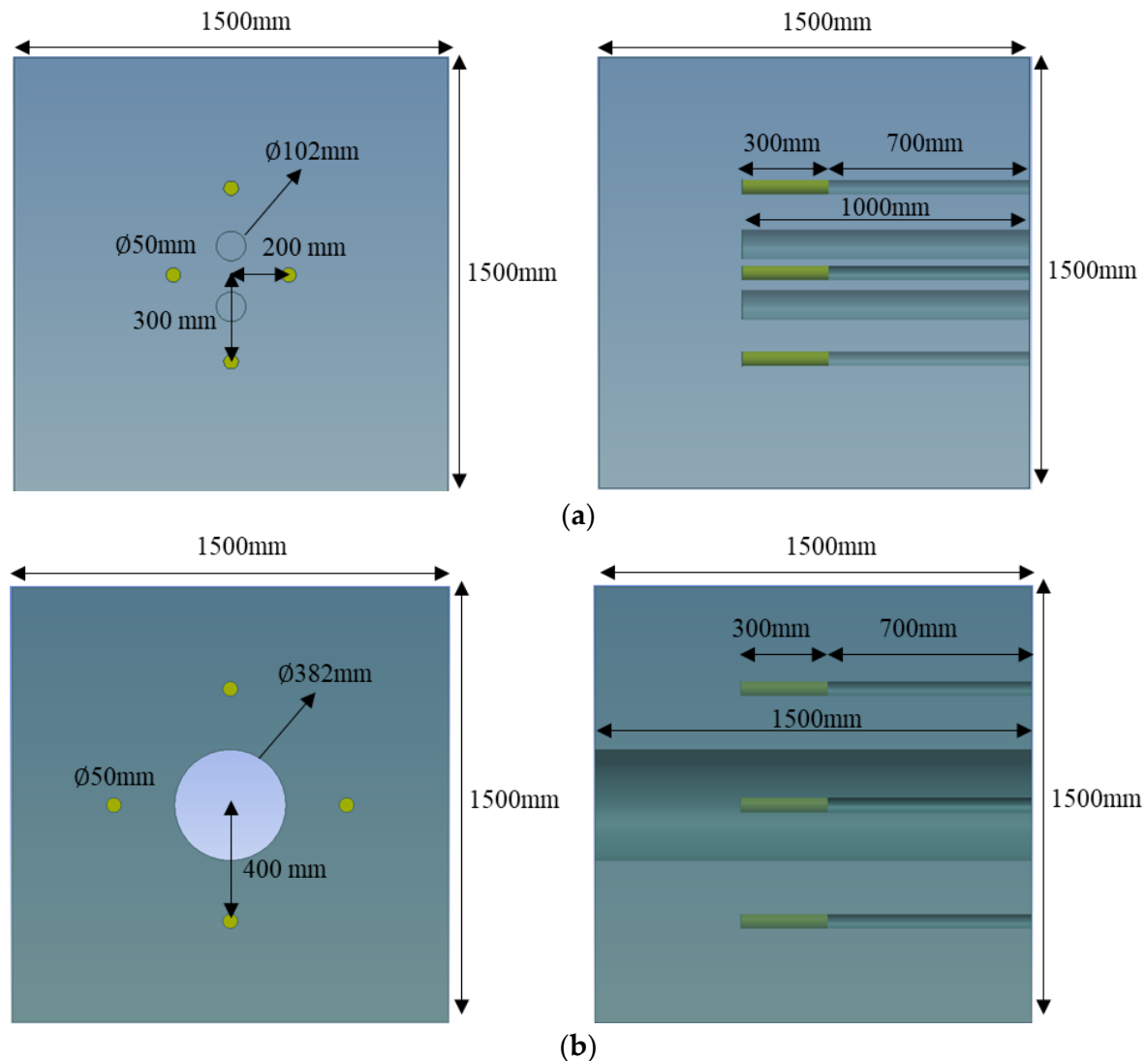


Figure 4. Geometry of numerical simulations for the burn-cut and the LLB methods. (a) Burn-cut method; (b) LLB method.

Table 1. Input parameter for JH-2 model in LS-DYNA.

Parameter	Value	Parameter	Value
Density (kg/m ³)	2560	Maximum normalized fractured strength	0.160
Shear modulus (GPa)	11.606	Hugoniot elastic limit (GPa)	4.500
Intact normalized strength parameter A	1.248	Pressure component at the Hugoniot elastic limit (GPa)	2.930
Fractured normalized strength parameter B	0.680	Fraction of elastic energy loss	1.000
Strength parameter C	0.005	Parameter for a plastic strain to fracture D_1	0.008
Fractured strength parameter M	0.830	Parameter for a plastic strain to fracture D_2	0.435
Intact strength parameter N	0.676	First pressure coefficient K1 (GPa)	10.720
Reference strain rate	1.000	Second pressure coefficient K2 (GPa)	−386
Maximum tensile strength (GPa)	0.015	Elastic constant K3 (GPa)	12,800

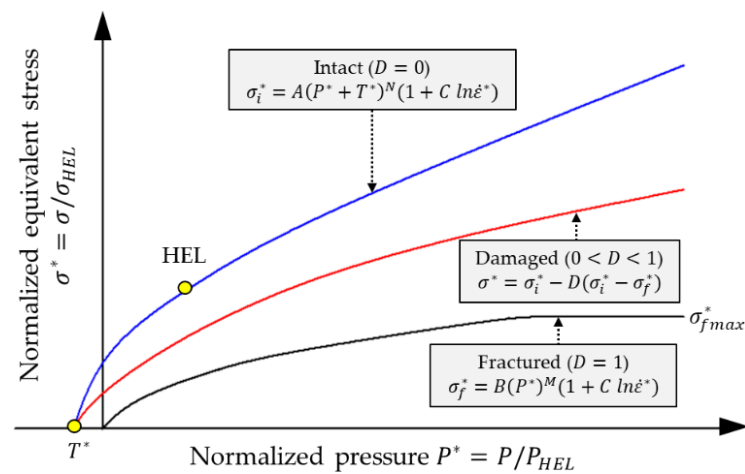


Figure 5. Strength model for the JH-2 constitutive model.

The JH-2 model includes the following three types of strength: intact state, damaged state, and fractured state, as shown in Figure 5. The three states have their own strength equations, which present the relationship between the normalized equivalent stress and the normalized pressure, expressed as

$$\sigma^* = \sigma_i^* - D(\sigma_i^* - \sigma_f^*) = \sigma / \sigma_{HEL} \quad (1)$$

where σ_i^* is the normalized intact equivalent stress, σ_f^* is the normalized fracture stress, D is the damage coefficient ($0 \leq D \leq 1$), σ is the actual equivalent stress calculated by the von Mises stress formula, and σ_{HEL} is the equivalent stress at the Hugoniot elastic limit (HEL). The HEL stands for the net compressive stress at which a one-dimensional shock wave with uniaxial strain exceeds the elastic limit of the material. The brittle material begins to soften when the damage begins to accumulate, and this process can be expressed by Equation (1). Although the softening does not continue when the material is completely damaged ($D = 1$), it allows for gradual softening of the brittle material under increasing plastic strain. The normalized intact strength and fracture strength are given by

$$\sigma_i^* = A(P^* + T^*)^N (1 + C \times \ln \dot{\epsilon}^*) \quad (2)$$

$$\sigma_f^* = B(P^*)^M (1 + C \times \ln \dot{\epsilon}^*) \quad (3)$$

where A , B , C , M , and N are all constants. The normalized pressure is $P^* = P/P_{HEL}$, where P is the actual pressure and P^* is the pressure at the HEL. The normalized maximum tensile hydrostatic pressure is $T^* = T/P_{HEL}$, where T is the maximum tensile hydrostatic pressure. The strain is $\dot{\epsilon}^* = \dot{\epsilon}/\dot{\epsilon}_0$, where $\dot{\epsilon}$ is the actual strain; $\dot{\epsilon}_0 = 1 \text{ s}^{-1}$ is the reference strain rate.

The damage is mainly accumulated due to the generation of fractures, and the damage graph is shown in Figure 6a. The damage in the JH-2 model can be expressed as follows:

$$D = \sum \Delta \epsilon^p / \epsilon_f^p = \sum \Delta \epsilon^p / [D_1(P^* + T^*)^{D_2}] \quad (4)$$

where $\Delta \epsilon^p$ is the plastic strain during a cycle of integration, ϵ_f^p is the plastic strain to the fracture under constant pressure P , and D_1 and D_2 are the damage factors for ϵ_f^p . The equation of state (EOS) for the JH-2 constitutive model, as shown in Figure 6b, presents the relationship between hydrostatic pressure and volumetric strain, which consists of a pure elastic stage and a plastic damage stage. The hydrostatic pressure before the fracture and after the damage starts to accumulate can be expressed as follows:

$$P = K_1 \mu + K_2 \mu^2 + K_3 \mu^3 \dots (D = 0) \quad (5)$$

$$P = K_1\mu + K_2\mu^2 + K_3\mu^3 + \Delta P \dots (0 < D < 1) \tag{6}$$

where K_1 , K_2 , and K_3 are constants (K_1 is the bulk modulus), and $\mu = \rho/\rho_0 - 1$ for the current density ρ and the initial density ρ_0 . When the fracture occurs in the material, which is caused by the bulking energy, the incremental pressure ΔP is added. In this analysis model, erosion was set to occur when the tensile stress exceeds the maximum tensile strength of the rock mass, using blasting to simulate the rock failure.

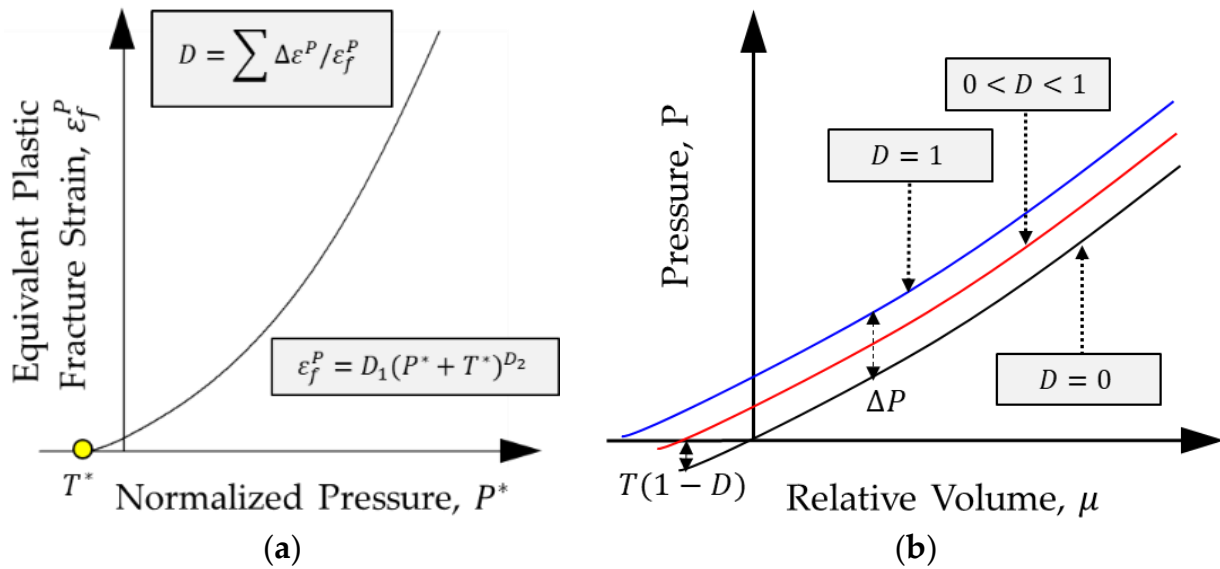


Figure 6. Damage and EOS models for the JH-2 constitutive model. (a) Damage model; (b) EOS model.

3.3. Explosive and Stemming Material Models

To model the pressure generated by the expansion of the detonation product, a Jones–Wilkins–Lee (JWL) equation of state (EOS) was used [34]. The JWL EOS is widely used in explosives modeling for describing the relationship of pressure–volume–energy for detonation products. In this study, JWL EOS was used to simulate the blasting process, and this equation can be expressed as follows:

$$P = A \left(1 - \frac{\omega}{R_1 V}\right)^{-R_1 V} + B \left(1 - \frac{\omega}{R_2 V}\right)^{-R_2 V} + \frac{\omega}{V} E_0 \tag{7}$$

where P is pressure, E and V are the detonation energy per unit volume and the relative volume, and A , B , R_1 , R_2 , and ω are the EOS coefficients, respectively. A high explosive burn (HEB) material card was used to simulate the detonation of the explosives. The input values for JWL EOS and HEB for an emulsion material are provided in Table 2 [35].

Table 2. Input parameter for JWL EOS in LS-DYNA.

JWL	Parameter	A	B	R_1	R_2	ω	E_0	V_0
	Value	(GPa)	(GPa)				(GPa/m ³ /m ³)	(m ³ /m ³)
		276	8.44	5.215	2.112	0.501	3.868	1.0
HEB	Parameter	RO	D		P_{cj}			
	Value	(kg/m ³)	(m/s)	(m/s)	(GPa)			
		1180	5122	5122	9.530			

where RO , D , and P_{cj} are the density, detonation velocity, and Chapman–Jouguet pressure, respectively.

Stemming is a material used to prevent the release of detonation gases by filling the remaining areas in the blast hole, and it helps the pressure generated by the explosives to crush the rock efficiently. Here, the stemming material was modeled using the FHWA_SOIL material model developed by the U.S. Federal Highway Administration (FHWA) [36]. This

model is an isotropic material with damage, and it is effective at modeling the behavior of soil under the consideration of strain-softening, kinematic hardening, strain rate effects, element deletion, excess pore water effects, and stability with no soil confinement; the input parameters are listed in Table 3 [37–39].

Table 3. Input parameter for FHWA_SOIL model in LS-DYNA.

Parameter	Value	Parameter	Value
Density (kg/m ³)	2350	Eccentricity parameter	0.700
Specific gravity	2.650	Moisture content	6.200
Density of water (kg/m ³)	1000	Skeleton bulk modulus (MPa)	0.153
Viscoplasticity parameter V_n	1.100	Minimum internal friction angle (radians)	0.063
Viscoplasticity parameter γ_r	0.0	Volumetric strain at initial damage threshold	0.001
Maximum number of plasticity iterations	10.00	Void formation energy	10.00
Bulk modulus (MPa)	15.30	Strain hardening, percent of φ_{max} where non-linear effects start	10.00
Shear modulus (MPa)	19.50	Pore water effects on bulk modulus PWD1	0.0
Peak shear strength angle (radians)	0.420	Pore water effects on effective pressure PWD2	0.0
Cohesion (MPa)	0.011	Strain hardening, amount of non-linear effects	10.00

The uncharged holes were modeled using the NULL material card, and the void was modeled using the LINEAR_POLYNOMIAL EOS material card, which is given by

$$P = C_0 + C_1\mu + C_2\mu^2 + C_3\mu^3 + (C_4 + C_5\mu + C_6\mu^2)E \quad (8)$$

where C_0 , C_1 , C_2 , C_3 , C_4 , C_5 , and C_6 are constants, and $\mu = \rho/\rho_0 - 1$, which is the ratio of the current density to the initial density. The detailed parameters for air are given in Table 4.

Table 4. Material model and EOS parameter for air.

ρ (kg/m ³)	C_0	C_1	C_2	C_3	C_4	C_5	C_6	E_0 (MPa)
1.29	0.0	0.0	0.0	0.0	0.4	0.4	0.0	0.25

3.4. Results of Numerical Analyses

Figure 7 displays the results of numerical analyses for the burn-cut and LLB methods over time, and shows side views of the analysis models in the wireframe element mode for observing the state of fracturing around the blast holes inside the rock mass. The number of elements of the burn-cut and LLB methods was 6,800,190 and 6,816,395, respectively.

When the explosives detonate after 0 s, the high-temperature and high-pressure gases are generated by the four blast holes; thus, compressive fractures are generated near the blast holes, and the explosion energy is propagated in the form of a compressive stress wave to the rock mass [40,41]. The propagated compressive stress wave reaches the uncharged holes before it reaches the tunnel face because of the shorter burden. The compressive stress wave first reaches the surface of the uncharged holes, and then is reflected as a tensile wave that begins to crush the rock around the uncharged holes at 0.2 ms in both cases. At 0.2 ms, in the burn-cut method, the spacing between the explosives and the uncharged hole is shorter than that of the LLB method; thus, the crushed zone around the uncharged hole was wider than in the LLB method. Then, the crushed area near the uncharged holes gradually increases. At the same time, the continuously propagated stress wave finally reaches the tunnel face and the rock is crushed, due to the reflected tensile stress at 0.8 and 1.0 ms, respectively. The crushed zones continuously increase due to the high pressure and the reflected tensile stress generated by the uncharged holes and the tunnel face.

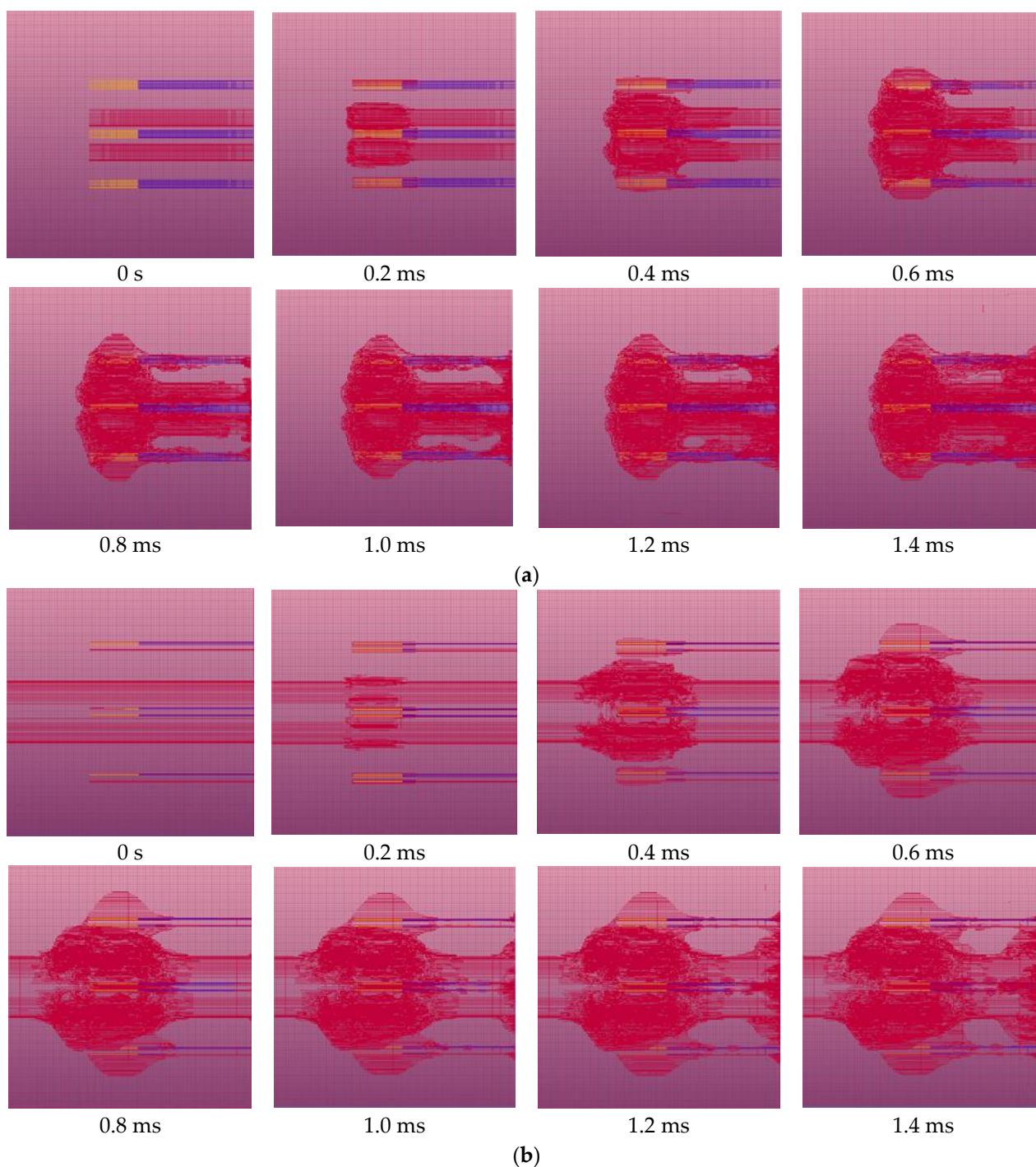


Figure 7. Results of the numerical analyses of the burn-cut and LLB methods. (a) Burn-cut method; (b) LLB method.

4. Discussion

4.1. Effect of Increasing the Advance Rate in the Burn-Cut and LLB Methods

Figure 8 summarizes the numerical analysis results at the last step (at 1.4 ms) to investigate the influence of the advance rate in the burn-cut and LLB methods. In the case of the Burn-cut method, the rock was crushed up to 0.09 m from the end line of the explosives, whereas the rock was crushed up to 0.37 m in the LLB method, which was more than four times the advance rate. It is believed that the large-diameter uncharged hole that was longer than the ordinary blast holes contributed significantly to the generation of more extensive tensile failure. In particular, in the burn-cut method, the blast-induced stress was

used more to crush rocks between the blast holes and the tunnel face than to increase the advance. On the other hand, blast-induced stress in the LLB method was used more to increase the advance. Therefore, the long and large-diameter uncharged hole is believed to contribute greatly to increasing the advance.

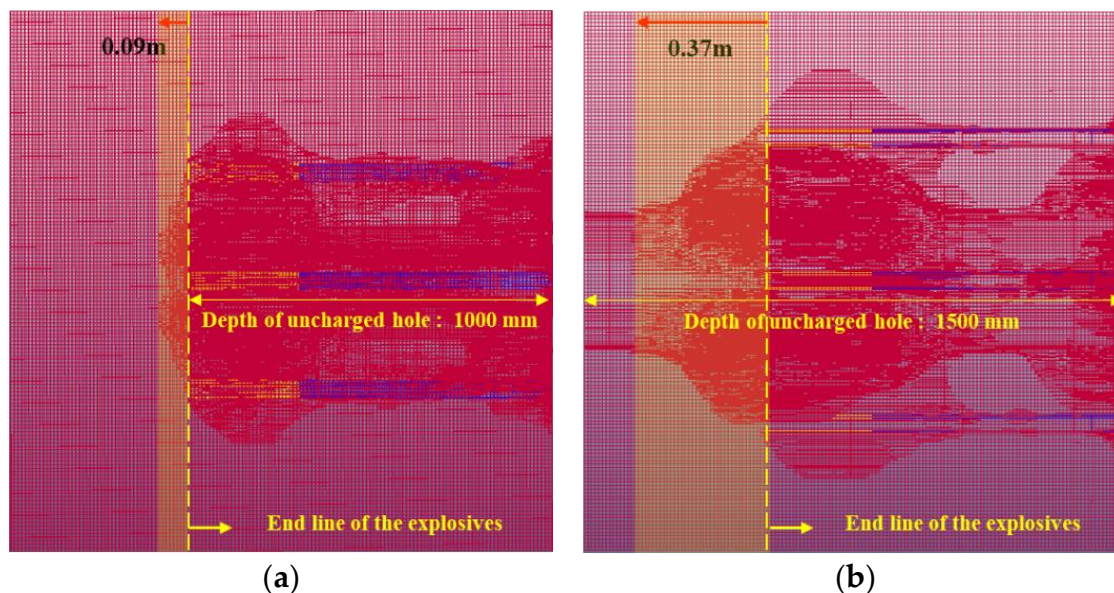


Figure 8. Comparison of the advance between the burn-cut and LLB methods. (a) Burn-cut method; (b) LLB method.

When explosives detonate near the cut area in the first stage, the long and large-diameter uncharged hole provides a larger space for crushed rock to move into, thus reducing the confining pressures of the surrounding rocks. Efficient moving of these crushed rocks creates an additional free face and reduces interference between the crushed rocks in the second stage. Considering that the entire blasting process uses the sequential blasting technique, which has a detonating delay time in the actual blasting, this method is significantly beneficial in that the long and large-diameter uncharged hole provides a larger space to move the crushed rocks into. In addition, the formed long and large-diameter uncharged hole before blasting provides an opportunity to reduce the amount of explosives; thus, the advance rate can be increased and the blast-induced vibration can be reduced.

4.2. Effect of Increasing the Advance in the Burn-Cut and LLB Methods

Additional analysis of the LLB method was carried out to investigate the blasting efficiency with the large-diameter uncharged hole with the same depth as the blast holes (a shorter depth than in the original LLB method). Figure 9 summarizes the results of the numerical analysis for the original LLB method and the modified LLB with a shorter uncharged hole. The number of elements of the modified LLB method was 6,719,248. The results show that the advance in the modified LLB method with its shorter uncharged hole was 0.11 m, which was approximately 3.36 times less than in the original LLB method. However, the advance in the modified LLB method was approximately 1.22 times longer than in the burn-cut method, as shown in Figure 8a. This suggests that the advance increased due to the long and large-diameter uncharged hole that caused a more extensive range of tensile failure compared to the burn-cut method. Given that the wider and longer uncharged hole significantly contributed to increasing the blasting efficiency as well as the advance, the LLB method has pronounced advantages compared to the traditional burn-cut method.

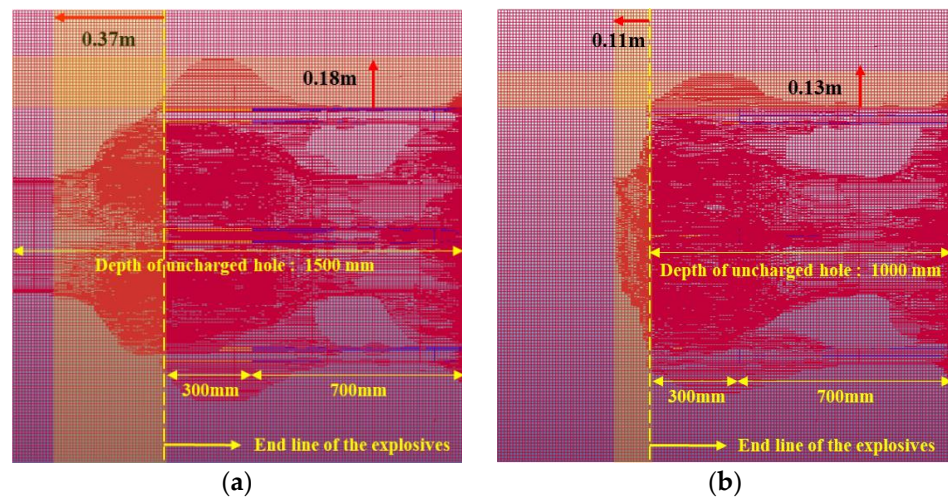


Figure 9. Comparison of blasting efficiency depending on the length of the large-diameter uncharged hole. (a) Original LLB method; (b) modified LLB method with reduced uncharged hole length.

4.3. Effect of Reducing the Amount of Explosives

Additional numerical analysis was performed to estimate the effect of reducing the amount of explosives when applying the LLB method. The total length of the explosives was reduced by 30%, from 300 to 210 mm, and the results are illustrated in Figure 10. The number of elements of the modified LLB method was 6,801,550. The crushed zone around the blast hole was about 2.25 times smaller than with the original LLB design, but the advance was similar, 0.37 mm compared to 0.36 mm with the original LLB design. Although the overall failure range decreased as the amount of explosives was decreased, the tensile failure caused by the long and large-diameter uncharged hole had a significant influence. Therefore, in sequential blasting, the modified LLB method with a reduced amount of explosives in the cut area can be expected to have similar blasting efficiency as the original LLB method.

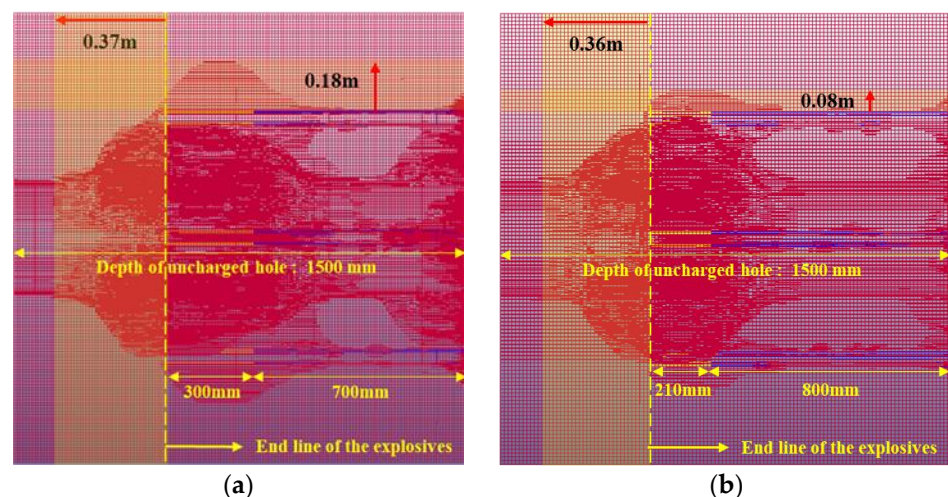


Figure 10. Comparison of failure zones depending on the amount of explosives in the LLB methods. (a) Total explosives length of 300 mm (original LLB method); (b) total explosives length of 210 mm (modified LLB method).

Figure 11 shows the numerical analysis results of blasting with the burn-cut method and the modified LLB method with a reduced amount of explosives. As mentioned above, although the total influence range near the explosives was decreased due to the reduction in the amount of explosives in the modified LLB method, its advance was four times longer

than that of the burn-cut method, as shown in Figure 11. Even in terms of blasting design, it is estimated that it is desirable to reduce the amount of explosives compared to the existing design, due to the large-diameter uncharged hole formed before blasting. Thus, the modified LLB method showed pronounced advantages in reducing blast-induced vibration by reducing the amount of explosives in the cut area, as well as increasing the advance.

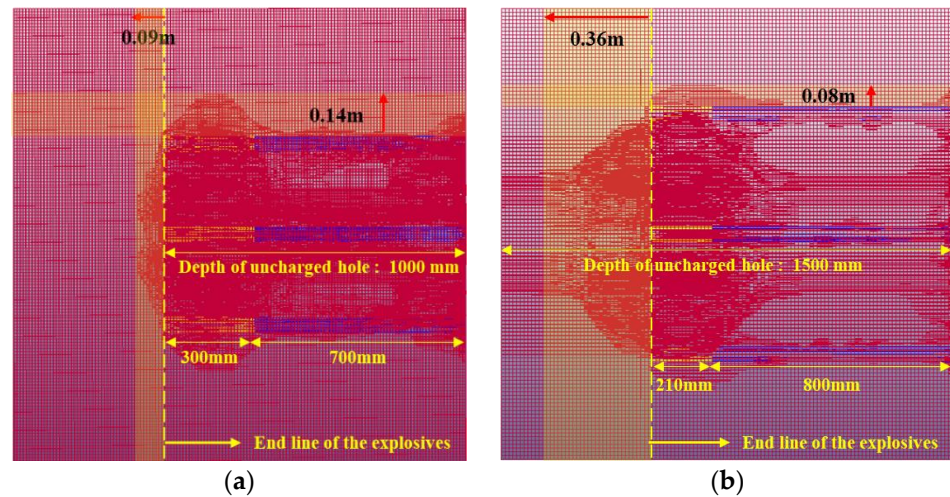


Figure 11. Comparison of range of failure in the burn-cut and the modified LLB methods. (a) Burn-cut method; (b) design of reduced explosives in the modified LLB method.

4.4. Comparison of Each Analysis Model using Eroding Elements

Figure 12 presents the total deleted eroding volume by detonation in the original LLB method, the burn-cut method, and the modified LLB method with reduced explosives. The total number of eroding elements can be used to compare the extent of the failure zones according to each method, and the number of deleted elements for each method was 101,953, 86,622, and 81,753, respectively. The original LLB method showed the widest range of the crushing zone, which was about 1.18 times larger than in the burn-cut method. In the modified LLB method with 30% reduced explosives, the total number of deleted eroding elements decreased by about 1.25 times compared to the original LLB, and was about 1.06 times lower than the burn-cut method. The modified LLB method showed similar failure patterns compared to the original LLB method, but the number of deleted eroding elements around the blast holes decreased as the amount of explosives decreased. The main effect of the burn-cut method was the reduction in the failure zone between the blast holes and the tunnel face, rather than contributing to increasing the advance.

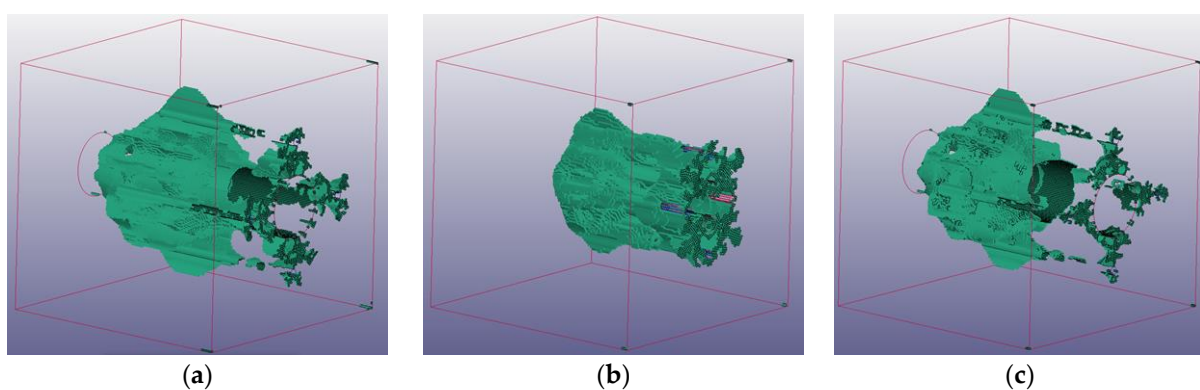


Figure 12. Comparison of deleted elements for each analysis model. (a) Original LLB method; (b) burn-cut method; (c) modified LLB method with reduced explosives.

In summary, the reduction in explosives in the modified LLB method reduced the overall size of the failure zones, but had a substantial advantage in that it contributed significantly to increasing the advance rate. Therefore, the LLB method clearly had better crushing efficiency than the traditional burn-cut method and, even when the amount of explosives in the cut area was reduced, this method had similar blasting efficiency compared to the traditional burn-cut method. Therefore, the modified LLB method can be considered an excellent alternative blasting method in that it not only reduces blast-induced vibration by reducing the amount of explosives needed in the cut area, but also increases the advance rate. However, since this is the result of the analysis using computer simulation, numerous field tests should be carried out for validation of the results.

5. Conclusions

In this study, numerical analysis using LS-DYNA software was performed to investigate the blast mechanism and efficiency by applying an advanced LLB cut blasting method that can effectively reduce blast-induced vibration. The Johnson–Holmquist (JH-2) constitutive model, which was developed for brittle materials subjected to dynamic conditions, was used to model the tunnel rock material, and the explosives and stemming materials were modeled using relevant emulsion and soil properties, respectively. The original LLB method was compared to the traditional burn-cut method as well as the modified LLB method, which shortened the depth of its large-diameter uncharged hole to match that of the blast holes and reduced the amount of explosives by 30%.

The numerical analysis confirmed that the new LLB method not only contributed to increasing the rock failure range in the cut area by forming an approximately 3.75 times larger uncharged hole than in the conventional burn-cut method, but also increased the advance rate by about 3.36 times by generating more tensile failure in the excavation direction. The modified LLB method used 30% less explosives and produced about 1.25 times fewer deleted eroding elements than the original LLB method (and 1.06 times fewer than the burn-cut method). In the traditional burn-cut method, which uses relatively small-diameter uncharged holes, explosives are used in crushing rocks more finely instead of contributing to increasing the advance rate. In contrast, the modified LLB method, with its long and large-diameter uncharged hole, generated more tensile failure in the excavation direction, so its advance rate increased four-fold compared to the burn-cut method. The long and large-diameter uncharged hole, which was already formed before blasting, reduces the initial confining stress of rock mass and can efficiently utilize the free face effect, thereby reducing the amount of explosives. Therefore, the modified LLB method, with its reduced amount of explosives, is significantly beneficial as an alternative method for reducing blast-induced vibration and increasing blasting efficiency, particularly in terms of advance per round, compared to the traditional burn-cut method. If a multi-LLB method that uses several long and large-diameter uncharged holes instead of one hole is considered, the blasting efficiency would increase significantly. Therefore, based on the numerical analysis, this method can be considered as an economical and eco-friendly blasting method for reducing the overall construction period and addressing environmental concerns.

Author Contributions: Conceptualization, S.S.L.; Data curation, M.-S.K.; Formal analysis, M.-S.K.; Funding acquisition, S.S.L.; Investigation, S.S.L.; Methodology, S.S.L.; Project administration, S.S.L.; Resources, M.-K.S.; Software, M.-S.K.; Supervision, S.S.L.; Validation, C.-Y.K.; Visualization, M.-S.K.; Roles/Writing—original draft, M.-S.K.; Writing—review and editing, S.S.L. All authors have read and agreed to the published version of the manuscript.

Funding: This work was supported by a Korea Agency for Infrastructure Technology Advancement (KAIA) grant funded by the Ministry of Land, Infrastructure, and Transport (grant 22UUTI-C157786-03).

Institutional Review Board Statement: Not applicable.

Informed Consent Statement: Not applicable.

Data Availability Statement: Some or all data that support the findings of this study are available from the corresponding author upon reasonable request.

Conflicts of Interest: The authors declare that they have no known competing financial interest or personal relationship that could have appeared to influence the work reported in this paper.

References

1. New, B.M. Ground vibration caused by construction works. *Tunn. Undergr. Space Technol.* **1990**, *5*, 179–190. [[CrossRef](#)]
2. Berta, G. Blasting-induced vibration in tunneling. *Tunn. Undergr. Space Technol.* **1994**, *9*, 175–187. [[CrossRef](#)]
3. Singh, P.K.; Vogt, W. Effect of direction of initiation on ground vibrations. *Int. J. Min. Reclam.* **1998**, *12*, 75–78. [[CrossRef](#)]
4. Singh, T.N.; Singh, V. An intelligent approach to prediction and control ground vibration in mines. *Geotech. Geol. Earthq. Eng.* **2005**, *23*, 249–262. [[CrossRef](#)]
5. Lu, C.P.; Dou, L.M.; Wu, X.R.; Xie, Y.S. Case study of blast-induced shock wave propagation in coal and rock. *Int. J. Rock Mech. Min. Sci.* **2010**, *47*, 1046–1054. [[CrossRef](#)]
6. Kuzu, C.; Guclu, E. The problem of human response to blast induced vibrations in tunnel construction and mitigation of vibration effects using cautious blasting in half-face blasting rounds. *Tunn. Undergr. Space Technol.* **2009**, *24*, 53–61. [[CrossRef](#)]
7. Ainalis, D.; Kaufmann, O.; Tshibangu, J.P.; Verlinden, O.; Kouroussis, G. Modelling the source of blasting for the numerical simulation of blast-induced ground vibrations: A review. *Rock Mech. Rock Eng.* **2017**, *50*, 171–193. [[CrossRef](#)]
8. Mesec, J.; Kovac, I.; Soldo, B. Estimation of particle velocity based on blast event measurements at different rock units. *Soil Dyn. Earthq. Eng.* **2010**, *30*, 1004–1009. [[CrossRef](#)]
9. Yan, Y.; Hou, X.M.; Fei, H.L. Review of predicting the blast-induced ground vibrations to reduce impacts on ambient urban communities. *J. Clean Prod.* **2020**, *260*, 121135–121155. [[CrossRef](#)]
10. Kim, M.S.; Lee, S.S. The efficiency of large hole boring (MSP) method in the reduction of blast-induced vibration. *Appl. Sci.* **2021**, *11*, 1814. [[CrossRef](#)]
11. Beak, J.H.; Beak, S.H.; Han, D.H.; Won, A.R.; Kim, C.S. A study on the design of PLHBM. *Explos. Blasting.* **2012**, *30*, 66–76.
12. Ma, G.W.; An, X.M. Numerical simulation of blasting-induced rock fractures. *Int. J. Rock Mech. Min. Sci.* **2008**, *45*, 966–975. [[CrossRef](#)]
13. Qui, X.Y.; Hao, Y.; Shi, X.; Hao, H.; Zhang, S.; Gou, Y. Numerical simulation of stress wave interaction in short-delay blasting with a single free surface. *PLoS ONE.* **2018**, *13*, e0204166. [[CrossRef](#)]
14. Jeong, H.Y.; Jeon, B.K.; Choi, S.B.; Jeon, S.W. Fracturing behavior around a blasthole in a brittle material under blasting loading. *Int. J. Impact Eng.* **2020**, *140*, 103562–103576. [[CrossRef](#)]
15. Zhang, H.; Li, T.C.; Du, Y.T.; Zhu, Q.W.; Zhang, X.T. Theoretical and numerical investigation of deep-hole cut blasting based on cavity cutting and fragment throwing. *Tunn. Undergr. Space Technol.* **2021**, *111*, 103854–103871. [[CrossRef](#)]
16. Yang, Y.Z.; Shao, Z.S.; Mi, J.F.; Xiong, X.F. Effect of adjacent hole on the blast-induced stress concentration in rock blasting. *Adv. Civ. Eng.* **2018**, *3*, 5172878. [[CrossRef](#)]
17. Kutter, H.K.; Fairhurst, C. On the fracture process in blasting. *Int. J. Rock Mech. Min. Sci. Geomech. Abstr.* **1971**, *8*, 189–202. [[CrossRef](#)]
18. Esen, S.; Onederra, L.; Bilgin, H. Modelling the size of the crushed zone around a blasthole. *Int. J. Rock Mech. Min. Sci.* **2003**, *40*, 485–495. [[CrossRef](#)]
19. Hopkinson, B. A method of measuring the pressure produced in the detonation of high explosives or by the impact of bullets. *Philos. Trans. R. Soc. Lond. Ser. A* **1913**, *89*, 411–413. [[CrossRef](#)]
20. Kolsky, H. *Stress Waves in Solids*, 1st ed.; Courier Corporation: Oxford, UK, 1953.
21. Chai, S.B.; Li, J.C.; Zhang, Q.B.; Li, H.B.; Li, N.N. Stress wave propagation across a rock mass with two non-parallel joints. *Rock Mech. Rock Eng.* **2016**, *49*, 4023–4032. [[CrossRef](#)]
22. Oh, S.W.; Choi, B.H.; Min, G.J.; Jung, Y.B.; Cho, S.H. An experimental study on the dynamic increase factor and strain rate dependency of the tensile strength of rock materials. *Explos. Blasting* **2021**, *39*, 10–21.
23. Cho, S.H.; Ogata, Y.; Kaneko, K. Strain-rate dependency of the dynamic tensile strength of rock. *Int. J. Rock Mech. Min. Sci.* **2003**, *40*, 763–777. [[CrossRef](#)]
24. Li, X.H.; Zhu, Z.M.; Wang, M.; Shu, Y.; Deng, S.; Xiao, D.J. Influence of blasting load directions on tunnel stability in fractured rock mass. *J. Rock Mech. Geotech. Eng.* **2022**, *14*, 346–365. [[CrossRef](#)]
25. Yang, J.H.; Cai, J.Y.; Yao, C.; Li, P.; Jiang, Q.H.; Zhou, C.B. Comparative study of tunnel blast-induced vibration on tunnel surfaces and inside surrounding rock. *Rock Mech. Rock Eng.* **2019**, *52*, 4747–4761. [[CrossRef](#)]
26. Hu, Y.G.; Yang, Z.W.; Huang, S.L.; Lu, W.B.; Zhao, G. A new safety control method of blasting excavation in high rock slope with joints. *Rock Mech. Rock Eng.* **2020**, *53*, 3015–3029. [[CrossRef](#)]
27. Yin, Y.; Sun, Q.; Zou, B.P.; Mu, Q.Y. Numerical study on an innovative shaped charge approach of rock blasting and the timing sequence effect in microsecond magnitude. *Rock Mech. Rock Eng.* **2021**, *54*, 4523–4542. [[CrossRef](#)]
28. Souli, M.; Bouamoul, A.; Nguyen-Dang, T.V. Ale formulation with explosive mass scaling for blast loading: Experimental and numerical investigation. *Comput. Model Eng. Sci.* **2012**, *86*, 469–486. [[CrossRef](#)]

29. Olovsson, L.; Souli, M.; Do, I. LS-DYNA—ALE Capabilities (Arbitrary-Lagrangian-Eulerian) Fluid-Structure Interaction Modeling. Livermore Software Technology Corporation. 2003. Available online: <https://ftp.lstc.com/anonymous/outgoing/jday/aletutorial-278p.pdf> (accessed on 10 March 2022).
30. Johnson, G.R.; Holmquist, T.J. Response of boron carbide subjected to large strains, high strain rates, and high pressures. *J. Appl. Phys.* **1999**, *85*, 8060–8073. [[CrossRef](#)]
31. Holmquist, T.J.; Johnson, G.R. Response of silicon carbide to high velocity impact. *J. Appl. Phys.* **2002**, *91*, 5858–5866. [[CrossRef](#)]
32. Wang, J.X.; Yin, Y.; Esmaili, K. Numerical simulations of rock blasting damage based on laboratory-scale experiments. *J. Geophys. Eng.* **2018**, *15*, 2399–2417. [[CrossRef](#)]
33. Wang, J.X.; Yin, Y.; Lu, C.W. Johnson–Holmquist-II(JH-2) constitutive model for rock materials: Parameter determination and application in tunnel smooth blasting. *Appl. Sci.* **2018**, *8*, 1675. [[CrossRef](#)]
34. Lee, E.L.; Horning, H.C.; Kury, J.W. *A Diabatic Expansion of High Explosives Detonation Products*; TID4500-UCRL 50422; Lawrence Livermore National Laboratory, University of California: Livermore, CA, USA, 1968.
35. Yi, C.P. *Improved Blasting Results with Precise Initiation—Numerical Simulation of Sublevel Caving Blasting*; Report; Swedish Blasting Research Centre: Stockholm, Sweden, 2013; Volume 3.
36. Lewis, B.A. *Manual for LS-DYNA Soil Material Model 147*; Federal Highway Administration: McLean, VA, USA, 2004.
37. Koneshwaran, S.; Thambiratnam, D.P.; Gallage, C. Blast response of segmented bored tunnel using coupled SPH-FE method. *Structure* **2015**, *2*, 58–71. [[CrossRef](#)]
38. Livermore Software Technology. *LS-DYNA Keyword User’s Manual—Volume II R12*; Livermore Software Technology: Livermore, CA, USA, 2020.
39. Baranowski, P.; Mazurkiewicz, L.; Malachowski, J.; Pytlik, M. Experimental testing and numerical simulations of blast-induced fracture of dolomite rock. *Meccanica* **2020**, *55*, 2338–2352. [[CrossRef](#)]
40. Cho, S.H.; Kaneko, K. Rock Fragmentation Control in Blasting. *Mater. Trans.* **2004**, *45*, 1722–1730. [[CrossRef](#)]
41. Shadabfar, M.; Gokdemir, C.; Zhou, M.L.; Kordestani, H.; Muho, E.V. Estimation of Damage Induced by Single-Hole Rock Blasting: A Review on Analytical, Numerical, and Experimental Solutions. *Energies* **2020**, *14*, 29. [[CrossRef](#)]